Burial of the polar magnetic field of an accreting neutron star and gravitational wave emission

D. J. B. Payne, M. Vigelius and A. Melatos

School of Physics, University of Melbourne, Parkville, VIC 3010

Abstract. We present detailed, ab initio numerical simulations of the distorted magnetic structure of an accreting neutron star as a function of accreted mass M_a: (i) we evolve an initial dipole through a quasi-static sequence of Grad-Shafranov equilibria while maintaining strict flux-freezing for the first time and (ii) we import these equilibria into the time-dependent, ideal-magnetohydrodynamic (MHD) code ZEUS-3D and load additional mass on to the star dynamically. We investigate the stability of these hydromagnetic equilibria by perturbing them in ZEUS-3D in two and three dimensions. Surprisingly, in both cases, the equilibria are marginally stable for all $M_a \leq 6 \times 10^{-4} M_\odot$. On extending the ZEUS-3D simulations to non-ideal MHD, preliminary results indicate that the equilibria are still not disrupted. The ohmic diffusion time-scale is $10^5 (10^2)$ times longer than the accretion time-scale in 2D (3D). The equilibria ("magnetic mountains") are in general, offset from the spin axis and thus generate gravitational waves. We show that the gravitational wave strain is detectable by Advanced LIGO even after Ohmic dissipation and 3D hydromagnetic instabilities are considered.

Keywords: neutron stars – x-ray binaries – gravitational waves
PACS: 97.60.Jd – 97.80.Jp – 04.30.-w

INTRODUCTION

Low-field neutron stars in binary systems with a history of accretion are observed to have a magnetic dipole moment μ which decreases monotonically with accreted mass, M_a [1, 2]. Several mechanisms have been proposed to explain the magnetic field reduction: (i) accelerated Ohmic decay [3, 4], where the electrical conductivity of the crust is reduced by accretion-induced heating; (ii) interactions between superfluid neutron vortices (carrying circulation) and superconducting fluxoids (carrying magnetic flux) as the star spins down [5, 6], and (iii) magnetic screening or burial [7, 8], where the currents generating the original magnetic field are partially neutralised by accretion-induced crustal currents.

Considering magnetic burial, we implement a numerical scheme [9] to solve for the equilibrium hydromagnetic configuration of the star, given an accreted mass M_a [8]. Matter is funnelled to the magnetic poles and piles up in *magnetic mountains* until the hydrostatic pressure overcomes the magnetic tension at the mountain's base, causing it to spread sideways. The pinched, flaring geometry of the mountain is clear in Fig. 1. The equilibria are calculated up to $M_a \lesssim 10^{-4} M_\odot$, short of the mass required ($\sim 0.1 M_\odot$) to spin up a neutron star to millisecond periods. The equilibria contain steep field gradients and are thus subject to a plethora of instabilities which we probe with ZEUS-3D for both axisymmetric [10] and nonaxisymmetric equilibria [11], in the ideal- and non-ideal-MHD regimes.

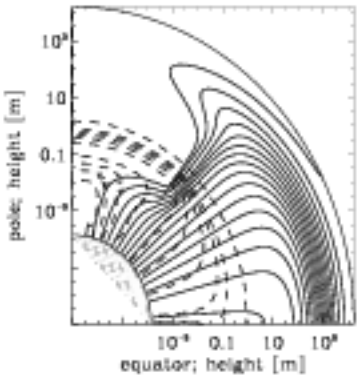

FIGURE 1. Polar plot of an axisymmetric magnetic mountain showing magnetic field lines (solid) and density contours (dashed) for $M_a = 10^{-5} M_\odot$. Altitude is marked on the axes (log scale) (from Ref. [8]).

The spin frequencies f_s of millisecond pulsars (accreting and radio) cut off sharply above $f_s \approx 0.7$ kHz, well below the centrifugal break-up frequency [12]. It has been argued that in these systems braking the star at 0.7 kHz [13]. Magnetic mountains are a viable source of the mass quadrupole required to achieve this [14].

AXISYMMETRIC EQUILIBRIA

The steady-state ideal-magnetohydrodynamic (MHD) equations for an isothermal atmosphere ($p = c_s^2 \rho$) reduce to the force equation

$$\nabla p + \rho \nabla \phi - \mu_0^{-1} (\nabla \times \mathbf{B}) \times \mathbf{B} = 0, \tag{1}$$

where $\mathbf{B}$ denotes magnetic field, ρ mass density, p pressure, and ϕ gravitational potential. For an axisymmetric configuration, we obtain the Grad-Shafranov equation [8]. To close the problem, and connect the initial and final states uniquely, we enforce the ideal-MHD constraint that mass is confined within in flux tubes, mainly closest to the magnetic poles. For the boundary conditions, we fix $\mathbf{B}$ to be dipolar at the stellar surface (line-tying), assume north-south symmetry, and let the field be free far from the star. The equations are solved numerically using an iterative scheme [9]. Convergence to the final state occurs monotonically for $M_a < 10^{-5} M_\odot$ but is more erratic for larger M_a. We also solve the problem analytically by a Green-function method in the small-M_a limit by way of verification.

STABILITY

Distorted magnetic configurations, in which the polar flux is buried beneath the accreted overburden, are expected to be unstable. However, in a sequence of two- and three-dimensional ZEUS-3D simulations, we have failed to disrupt our magnetic mountain equilibria. This is because, in the presence of line tying at the surface, the Grad-

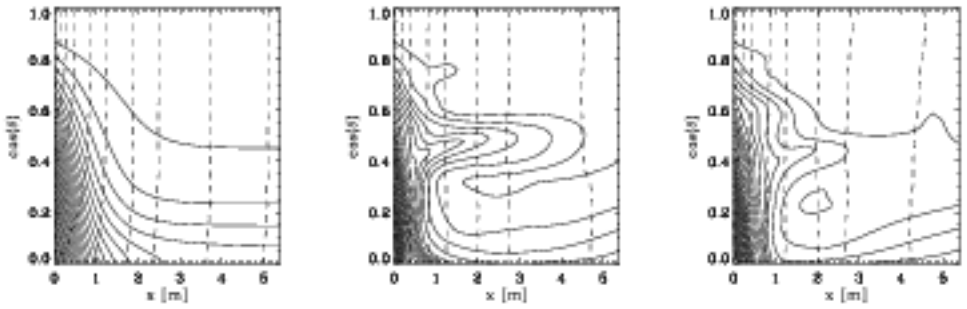

FIGURE 2. Evolution of the Parker instability for $M_a = 10^{-5} M_\odot$, with the density uniformly increased five-fold. Snapshots are taken at $t/\tau_A = 0, 200, 280$, where τ_A is the Alfvén time.

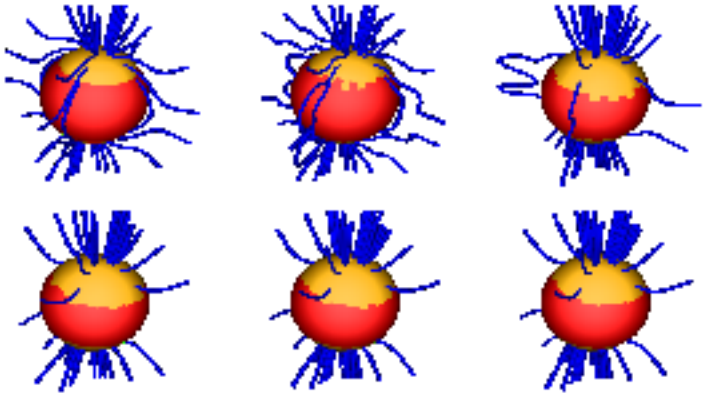

FIGURE 3. Evolution of the magnetic mountain ($M_a = 10^{-5} M_\odot$) in 3D at $t/\tau_A = 0,1,2,3,4,5$ (left to right, top to bottom). The mountain is defined by the isosurface $\rho = 1.03 \times 10^6 \mathrm{g\,cm^{-3}}$ and scaled up five-fold for clarity [11].

Shafranov equilibria represent final, saturated states of a nonlinear Parker (magnetic Rayleigh-Taylor) instability, reached quasistatically as accreted material is added. The Parker instability is observed transiently in ZEUS-3D (Fig. 2) when the density is uniformly increased across the grid [10]. As shown in Fig. 2, the Parker blister subsides and a new equilibrium state is reached with $< 1\%$ mass and flux loss overall.

On loading the axisymmetric Grad-Shafranov equilibrium (Fig. 1) into ZEUS-3D, perturbing it, and evolving it forward in time, we find that the mountain oscillates as sound and Alfvén waves propagate through it [10]. The mass quadrupole moment oscillates about its mean value, as is apparent in the series of snapshots shown in Fig. 3. Clearly the equilibrium is not disrupted. The Alfvén frequency varies with accreted mass $f_A \sim 17 (M_a/M_c)^{-1/2}$ Hz, while the sound frequency is fixed at $f_S \sim 0.4$ kHz [10].

On loading the Grad-Shafranov equilibrium state and allowing full 3D evolution, we observe a magnetic buoyancy instability, which introduces a toroidal component to the magnetic field ($\sim 10^{-7}$ the dipole field) after $200\tau_A$ (see Fig. 3). Again, after this transition phase, the system settles down to a new, nearly axisymmetric state (about the

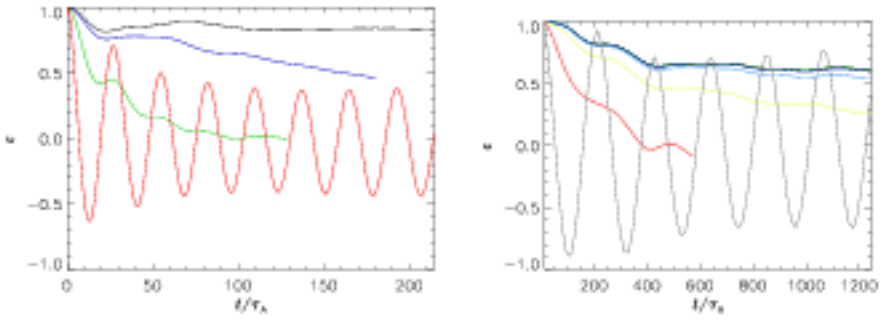

FIGURE 4. Evolution of the mass quadrupole moment in non-ideal MHD for $\tau_D/\tau_A = 10^{21}, 10^6, 10^5$, and 10^2 in 2D (left) and $10^{19}, 10^9, 10^7, 10^6, 10^5, 10^4, 10^2$ in 3D (right) (top to bottom).

misaligned magnetic axis) without further disruption.

OHMIC DISSIPATION

Non-ideal-MHD is implemented in ZEUS-MP by extending the method of characteristics and constrained transport (MOCCT) [15]. A new plethora of resistive instabilities is introduced in non-ideal-MHD. (We do not allow for Hall currents in any simulations thus far.) The Ohmic diffusion time-scale τ_D on which resistive instabilities act exceeds the accretion time-scale τ_a, with $\tau_D/\tau_a \sim 10^6$ in 2D and $\tau_D/\tau_a \sim 10^2$ in 3D [11]. Hence this time-scale is short enough to disrupt the mountain during the lifetime of a millisecond pulsar ($\sim 10^9$ yr) only if $\tau_D < 10^6$ yr. We plot the mass ellipticity ε as a function of time in both two and three dimensions in Fig. 4. The resistive instability time-scale is defined as the time it takes for ε to reach half its initial value (e.g. $150\tau_A$ for $\tau_D/\tau_A = 10^6$ in 2D). In 3D, we use the non-axisymmetric end-state reached above as an initial state. The ZEUS-MP time-step in 3D is about eight-fold shorter than in 2D and hence an electron-phonon conductivity $\sigma = 7.6 \times 10^{26} s^{-1}$ [16], uniform across the grid, corresponds to $\tau_D/\tau_A = 10^{21}$ in 2D and 10^{19} in 3D. The oscillation period seen for very large resistivities is thus similar for both 2D and 3D. Importantly, ε decreases by 20% and 40% for 2D and 3D respectively as soon as any resistivity is introduced - a significant but not detramental disruption of the magnetic mountains.

GRAVITATIONAL WAVES

Rapidly rotating neutron stars are a prime candidate for gravitational-wave detection by long-baseline interferometers like the Laser Interferometer Gravitational-Wave Observatory (LIGO). They allow coherent matched filtering without a computationally expensive hierarchical Fourier search [17] as they emit continuously at frequencies and sky positions that are, in principle, known a priori from X-ray timing. The spin frequencies f_s of accreting millisecond pulsars, measured from X-ray pulses and/or thermonuclear burst oscillations [12, 18], have a distribution that cuts off sharply above $f_s \approx 0.7$ kHz, well below the centrifugal break-up frequency for most nuclear equations of state [19]. This

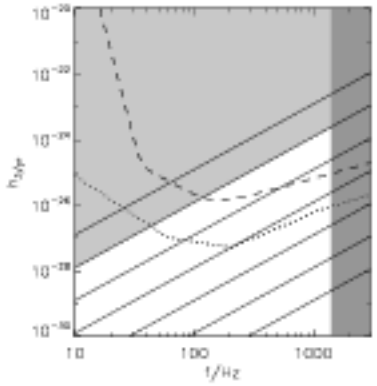

FIGURE 5. Polarization- and orientation-averaged gravitational wave strain h_c as a function of wave frequency f_s showing the noise curves for Initial (dashed) and Advanced (dotted) LIGO. Theoretical curves are overlaid for varying M_a, from 10^{-8} (lowest) to 10^{-2} (highest). Frequencies above $2f_s = 1.4$ kHz are shaded (dark, right). Mountain quadrupoles limited by Ohmic spreading are also shaded (light).

can be explained if a gravitational-wave torque balances the accretion torque, provided that the ellipticity satisfies $\varepsilon \sim 10^{-8}$ [13]. Several mechanisms of producing such ellipticities have been proposed including temperature gradients [13], large toroidal magnetic fields in the stellar interior [20], and polar magnetic burial [16, 14, this work].

Initial LIGO has have already set upper limits on ε for isolated radio pulsars, reaching as low as $\varepsilon \leq 4.5 \times 10^{-6}$ for J2124−3358. Figure 5 shows the LIGO noise curves overlaid with the calculated signal for different values of M_a. Global MHD oscillations of the mountain (see above), whether natural or stochastically driven, act to modulate the gravitational wave signal, creating sidebands in the frequency spectrum around f_s and $2f_s$. The signal-to-noise ratio (SNR) achieved by LIGO with coherent matched filtering can be enhanced by up to 15%, depending on where f_s lies relative to the noise curve minimum (Fig. 5). We find SNR ~ 3 for $f_s = 0.6$ kHz [14].

DISCUSSION

Magnetic mountains forming during polar accretion onto a neutron star are stable when perturbed and allowed to evolve in ZEUS-3D in ideal MHD. The mountains are calculated with a Grad-Shafranov iterative algorithm, which produces equilibria which are saturated, nonlinear, final states of the Parker instability. Transient Parker instabilities are seen in ZEUS-3D before new stable equilibria are reached. Resistive instabilities act on time-scales longer than the accretion time-scale in both two and three dimensions. The mountains are offset generally from the spin axis and produce gravitational radiation, spread around f_s and $2f_s$ by MHD oscillations. This signal is potentially detectable by laser-interferometer gravitational-wave detectors such as LIGO. Computation of templates for use with LIGO data are under way [21].

Our analysis applies to a biaxial star whose principal axis of inertia coincides with the magnetic axis and is thus generally inclined with respect to the angular momentum axis.

Such a star precesses [22], a fact neglected thus far and discussed further by Payne and Melatos [14]. To compute the polarization waveforms with precession included, one can employ the small-wobble-angle expansion for a nearly spherical star [23, 24].

Magnetic burial predicts the magnetic dipole moment μ and ε as a function of M_a. Eliminating M_a gives a direct relation $\varepsilon(\mu)$ and thus $h_c(\mu)$ (h_c is wave strain). Once gravitational waves are detected, these relations motivate observational tests for the burial model. In addition, the equilibria have a strong equatorial magnetic belt which can inhibit heat transport (and thus thermonuclear burst spreading) by conduction, convection, radiation, and ageostrophic shear [25]. This may explain the persistence and highly sinusoidal profile of oscillations observed in the tails of type I X-ray bursts in low-mass X-ray binaries [26].

REFERENCES

1. R. E. Taam, and E. P. J. van den Heuvel, *ApJ* **305**, 235–245 (1986).
2. E. P. J. van den Heuvel, and O. Bitzaraki, *A&A* **297**, L41 (1995).
3. V. Urpin, and U. Geppert, *MNRAS* 275, 1117–1124 (1995).
4. V. Urpin, and D. Konenkov, *MNRAS* 284, 741–748 (1997).
5. A. G. Muslimov, and A. I. Tsygan, *SvAL* 11, 80 (1985).
6. G. Srinivasan, D. Bhattacharya, A. Muslimov, and A. Tsygan, *Curr. Sci.* **59**, 31 (1990).
7. J. M. Blondin, and K. Freese, *Nature* 323, 786–788 (1986).
8. D. J. B. Payne, and A. Melatos, *MNRAS* 351, 569–584 (2004).
9. T. Mouschovias, *ApJ* **192**, 37–50 (1974).
10. D. J. B. Payne, and A. Melatos, *MNRAS* 376, 609–624 (2007).
11. M. Vigelius, and A. Melatos, *MNRAS, in prep.* (2007).
12. D. Chakrabarty, E. H. Morgan, M. P. Muno, D. K. Galloway, R. Wijnands, M. van der Klis, and C. B. Markwardt, *Nature* 424, 42–44 (2003).
13. L. Bildsten, *ApJL* **501**, L89 (1998).
14. D. J. B. Payne, and A. Melatos, *ApJ* **641**, 471–478 (2006).
15. C. Fendt, and M. Čemeljić, *A&A* **395**, 1045–1060 (2002).
16. A. Melatos, and D. J. B. Payne, *ApJ* **623**, 1044–1050 (2005).
17. P. R. Brady, T. Creighton, C. Cutler, and B. F. Schutz, *Phys. Rev. D* 57, 2101–2116 (1998).
18. R. Wijnands, M. van der Klis, J. Homan, D. Chakrabarty, C. B. Markwardt, and E. H. Morgan, *Nature* 424, 44–47 (2003).
19. G. B. Cook, S. L. Shapiro, and S. A. Teukolsky, *ApJL* 423, L117 (1994).
20. C. Cutler, *Phys. Rev. D* **66**, 084025 (2002).
21. C. Chung, and A. Melatos, *MNRAS, in prep.* (2007).
22. C. Cutler, and D. I. Jones, *Phys. Rev. D* **63**, 024002 (2001).
23. M. Zimmermann, *Phys. Rev. D* 21, 891–898 (1980).
24. C. Van Den Broeck, *Classical and Quantum Gravity* 22, 1825–1839 (2005).
25. D. J. B. Payne, and A. Melatos, *ApJ* **652**, 597–602 (2006).
26. M. P. Muno, F. Özel, and D. Chakrabarty, *ApJ* 581, 550–561 (2002).